9ICEG

Experimental and numerical simulations for coupled thermo-hydro-mechanical processes considering pore air pressure evolution in a clay-based engineered barrier of geological repositories for radioactive waste

S. Yamamoto[1], M. Moriiwa[2], S. Sato[3], T. Shimura[4], T. Nishimura[5]

[1]Senior general manager, Dr. Eng., Obayashi Corporation, Tokyo, Japan, email: yamamoto.shuichi@obayashi.co.jp

[2]Chief Engineer, Obayashi Corporation, Tokyo, Japan, email: moriiwa.motoki@obayashi.co.jp

[3]Manager, PhD, Obayashi Corporation, Tokyo, Japan, email: sato.shin.ro@obayashi.co.jp

[4]General Manager, Obayashi Corporation, Tokyo, Japan, email: shimura.tomoyuki@obayashi.co.jp

[5]Professor, Ashikaga University, Ashikaga, Japan, email: nishimura.tomoyoshi@g.ashikaga.ac.jp

ABSTRACT

In order to study how the gas phase pressure (including vapor pressure) develops and affects coupled thermo-hydro-mechanical (THM) processes in the clay based engineered barrier system (EBS) of a deep geological repository for radioactive waste, a programme of laboratory and modelling studies has been performed. A laboratory column test using compacted bentonite was performed under isothermal conditions in conjunction with coupled THM simulations of re-saturation processes in the repository including representations of the host rock and the heat generating waste.

The main findings are as follows:

1. Air in the bentonite is compressed due to water intrusion into the unsaturated bentonite from the host rock. This induces a gradual development of the gas phase pressure in the bentonite.
2. The change in gas pressure is controlled by the water saturation development. Temperature changes amplify the change in gas pressure. However, advective gas flow towards the rock is not possible because of low mobility in the saturated bentonite near the rock.
3. Therefore air can only migrate out of the bentonite (to the rock) by diffusion of dissolved air away from waste towards the rock.
4. As the bentonite suction decreases with ongoing saturation and the amount of air decreases by diffusion and the gas pressure reaches a peak after a certain time.
5. The void ratio varies locally during saturation, however the mechanical effects to evolution of gas pressure and saturation are negligibly small if confinement of the barrier material is kept sufficient.

Keywords: coupled THM analysis, laboratory test, bentonite, geological disposal, vapor pressure

1   INTRODUCTION

The clay based engineered barrier system (EBS) of a deep geological disposal of radioactive waste repository is subjected to high temperatures at the interface with disposal canisters due to heat generation of the high level waste while pore water intrudes into the EBS from the surrounding geosphere in the early post closure period. The coupled thermo-hydro-mechanical (THM) processes occurring during re-saturation produce the so called initial state of the EBS for long term safety assessment. In particular development of pressure in gas phase such as vapor pressure could importantly affect coupled THM processes and hence the initial state of the saturated EBS. Great research efforts concerning coupled THM phenomena have been made through large scale in-situ tests in underground rock laboratories at Grimsel (https://www.grimsel.com/) and Mont Terri (https://www.mont-terri.ch/) in Switzerland, Meuse/Haute-Marne (https://meusehautemarne.andra.fr/) in France, Äspö (https://www.skb.com/) in Sweden and other sites. DECOVALEX (https://decovalex.org/) is an international collaborative research project for numerical modelling of coupled THM processes,

which has considered the results from several of these in-situ tests. Models developed in DECOVALEX have demonstrated reproducibility of coupled THM behaviour and suggest that not only the liquid phase but also the gas phase including vapor should be taken into account for better reproducibility (Garitte, 2017; Alcolea, 2019). In particular, results from the Full-scale Emplacement (FE) experiment at the Mont Terri URL show that relative humidity in the vicinity of waste (heater) strongly depends on whether the model considers the vapor gas phase or not (Alcolea, 2019). However, coupling phenomena with the gas phase and its impact to the EBS performance are insufficiently understood.

In this study, an isothermal laboratory column test under controlled HM conditions and coupled THM numerical simulations have been performed, simulating the re-saturation processes for a compacted bentonite EBS, on the assumption that there is a 1-dmensional flow of pore fluid and heat between the host rock and the waste. In the laboratory column test, water intrudes into the base of the partially saturated bentonite column through a porous filter from a water supply system at atmospheric pressure, while the water and gas tightness is structurally guaranteed at the upper end. The bottom end and the upper end represent the interfaces respectively to the host rock and the waste. The bentonite column is emplaced in a cylindrical stainless steel mold and is completely confined by stainless steel caps at both ends. Two pressure transducers are positioned along the lateral surface of the sample to monitor the pore pressure in upper and lower part of the sample. The pore pressure evolution has been monitored over two years and monitoring is still ongoing. Coupled HM analyses considering the behaviour of gas phase were performed using the numerical code Code_Bright (Olivella et al., 1996) to reproduce the air pressure evolution in the test. Once a good agreement between the simulation and laboratory column test results had been achieved, coupled THM analyses were then performed, assuming a constant temperature of 70 °C at the top, 25 °C at the bottom and no heat-flow (insulation) across the lateral surfaces.

2 LABORATORY COLUMN TEST

2.1 Test apparatus

The apparatus consists of pore pressure sensor, steel mold, two cover plates, glass burette, data logger and PC. The steel mold had an inner diameter of 38.0 mm, a height of 76.0 mm and a thickness of 17.0 mm, with specially prepared upper and bottom plates. Two pressure sensors were installed at on the sides of the mold, at 18.0 mm from the top and bottom boundaries. The pressure sensors are Honeywell A 105 as shown in Figure 1 (left) with a range of 500 psi (corresponding to 3.4 MPa), and accuracy of 0.5 % full scale, and hysteresis ±0.5 %. Porous metal plates are placed between the top surface of pressure sensor and the lateral surface of the sample as shown in Figure 1 (right). The top and bottom surfaces of the sample are in contact with porous stone discs emplaced in dry conditions within the cap plates. The bottom side is connected to a glass burette for measuring the change in absorbed water with a difference voltage sensor. The difference voltage sensor is able to measure the water absorbed into the sample with time. The measured data sets recorded to the data logger, and PC provided a display of the measured pressures on the sides of the sample for the upper and lower sensors.
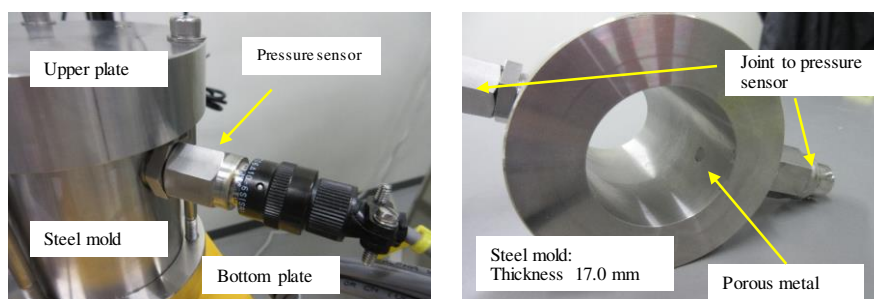

Figure 1. *Pressure sensor installed on the outside of the sample (left). P*orous metal equipped in the steel mold (right)

2.2 Test sample

This study used sodium bentonite (Kunigel V1). Owing to the significant high montmorillonite content, the bentonite had a fines content greater than 95 %. The bentonite was humidified by spraying deionized water to reach the desired initial water content, which was 10.0 % in this test. The samples had a

diameter of 38.0 mm and a height of 76.0 mm. The samples had the following initial physical properties: dry density of 1.200 Mg/m³, void ratio of 1.25, and saturation degree of 21.6 %. The size of the prepared sample was relatively small. A compression test was conducted to determine the pre-compression stress for the sample, and the variation of void ratio with compression stress as shown in Figure 2 (left). The compression index was estimated as 0.348 over the range 4.05 MPa to 35.7 MPa during the compression process. The sample for compression test was produced in the mold with a void ratio of 1.530, water content of 10.0 %, and applied vertical stress up to 35.7 MPa. The obtained compression curve gave a pre-compression stress 4.05 MPa when adjusting to void ratio of 1.250 corresponding to sample for measurement of pore pressure. The top surface of sample in the mold is shown in Figure 2 (right).
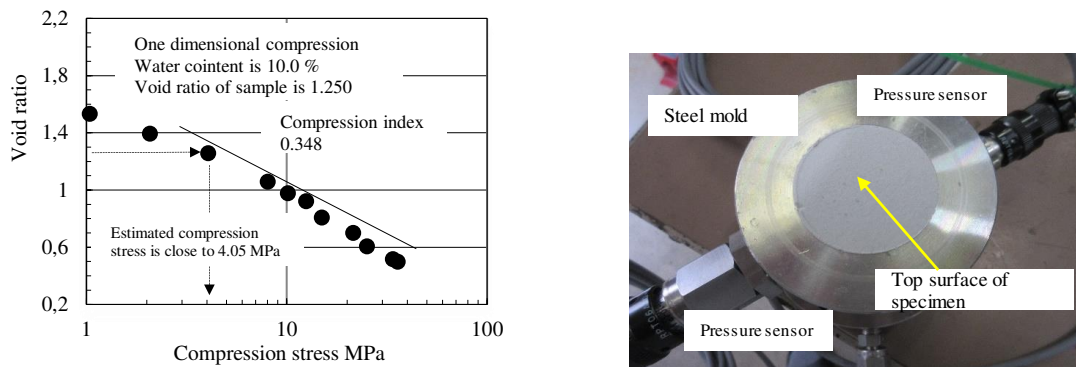

Figure 2. *Compression curve for bentonite (left). Sample in the steel mold with sensors (right)*

2.3   Test results and discussions

The pore pressures at the upper and lower sensors during the 767 days saturation period are shown in Figure 3. The upper and lower pore pressure sensors show a large increase over the first ten days. At the upper sensor the increase was maintained with constant gradient until 165 days, with a maximum pore pressure of 195.1 kPa. However, while the maximum pore pressure occurred in the upper part of the sample, the pore pressure in the bottom part indicated significantly smaller pressure than the upper part. The difference was 120 kPa. As mentioned below, it was possible to predict that swelling in the bottom part occurred due to hydration of the bentonite, as a high degree of saturation was achieved. Air in the bentonite pores was compressed due to the swelling induced by water intrusion from the base under the influence of the suction of the partially saturated bentonite. This induced a gradual development of the air pressure and pressure gradient according to the evolution of water saturation from the base of the sample. Following peak pore pressure, the pore pressure at the upper sensor showed a smooth reduction over time with an estimated gradient 0.19 kPa/day, lower than that during the increase in pressure (i.e., 1.11 kPa per day). As advective air flow due to the observed air pressure gradient is impossible because of the minimal gas mobility in the fully saturated bentonite at the bottom of the sample, the air can only migrate downward by diffusion of dissolved air from highly pressurized upper side to the water at low partial pressure in the bottom. This could be a reason for the very slow release of accumulated air pressure in the upper part. It is interesting that the pore pressures approach the same value after some time, indicating uniform pressure conditions in the sample. After 432 days the pore pressures at the lower sensor maintained at 100 kPa.

The hydration performance was considered from the change in average water content estimated from the total amount of absorbed water versus elapsed days, the resulting curve showed the asymptotic line shown in Figure 4 (left). A significant increase in water content is indicated at the beginning of test that continued over about 60 days. After this water content continues to smoothly increase and beyond 250 days the slope is 0.01 % per day until the end of test. Finally, the measured water content reached 45.5 % compared to the initial value of 10.0 %. The degree of saturation was calculated from the increasing water content shown in Figure 4 (right). The increase in degree of saturation is similar to that of the water content, and a value of 97.1 % is estimated at 767 elapsed days when the sample is approaching full saturation. It should be noted that the water content and saturation calculated from the loss of water from the burette are averages for the whole column. While the model values mentioned later are related to particular locations. The saturation of the test sample will be verified by post-mortem testing as a possible future verification step.

Considering the maximum pore pressure shown in Figure 3 together with the changing degree of saturation, the maximum pore pressure (195 kPa) measured at upper sensor at around 250 days. At that time the average degree of saturation had increased to 75.5 % and unsaturated conditions are assumed in the pore-space of the upper part of the sample. Once the sample was near fully saturated the pore pressure clearly decreased, and established a uniform pressure across the sample.
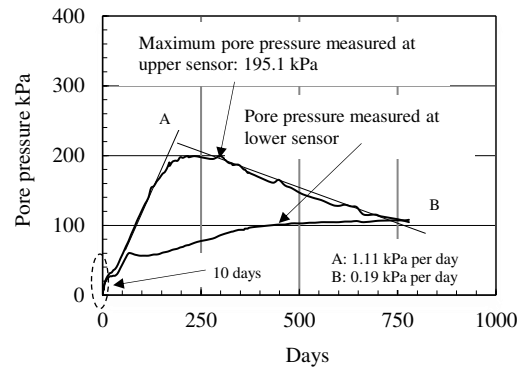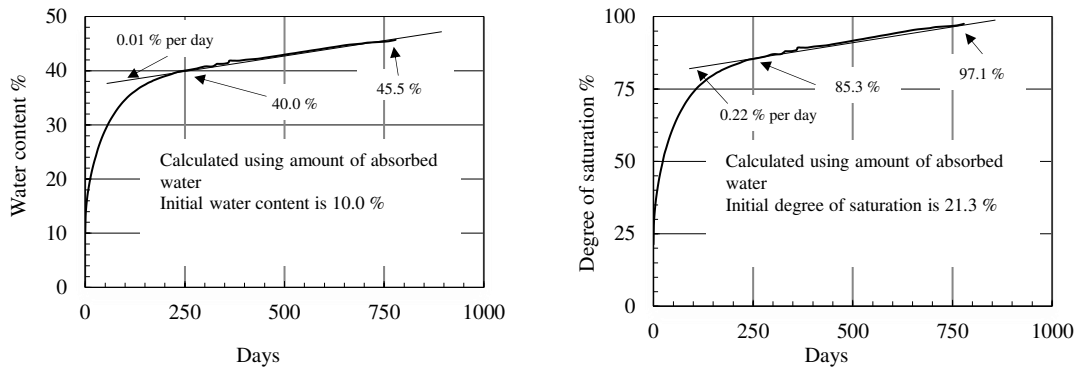
Figure 3. *Variation of pore pressures*

Figure 4. *Evolution of average water content (left). Evolution of sample saturation (right)*

3   NUMERICAL SIMULATION

3.1   Theory and method

The coupled HM and THM analyses incorporating two-phase flow were performed using the finite element code, Code_Bright (Olivella et al. 1996), which considers elastoplastic deformation such as swelling and consolidation of the bentonite, phase transformations of pore fluid (vaporization and dissolution of air), material properties depending on temperature, thermal expansion, permeability change with volumetric deformation. Here the hydromechanical behaviour of bentonite was represented using the Barcelona Basic Model (BBM: Alonso et al. 1990),

3.2   Modelling

3.2.1   Boundary and initial conditions

Figure 5 shows the axisymmetric finite element mesh and boundary and initial conditions used for the coupled HM analysis by Code_Bright. The right half space is modelled considering axisymmetric conditions. The dimensions of the model are the same as the column test sample. The boundary is mechanically free in the tangential direction and fixed in the normal direction. For the two phase flow boundary conditions, the top and side surfaces are impermeable to liquid and gas phases, and an atmospheric pressure at fully saturated condition is specified at the bottom. Diffusive outflow of dissolved air cannot be controlled for the bottom boundary conditions in the current version of Code_Bright and therefore out-diffusion at the bottom is not prevented in the analysis. All other boundary conditions of the analysis are the same as for the test. The initial conditions were set to those of the laboratory test.

Thermal boundary conditions were added for the coupled THM analysis. Fixed temperature boundaries of 25 °C at bottom and 70 °C at top were set. Temperature at the top was linearly increased up to constant 70 °C from an initial 25 °C to consider heating by a heater in the experiment. An adiabatic boundary condition is defined at lateral model boundary.
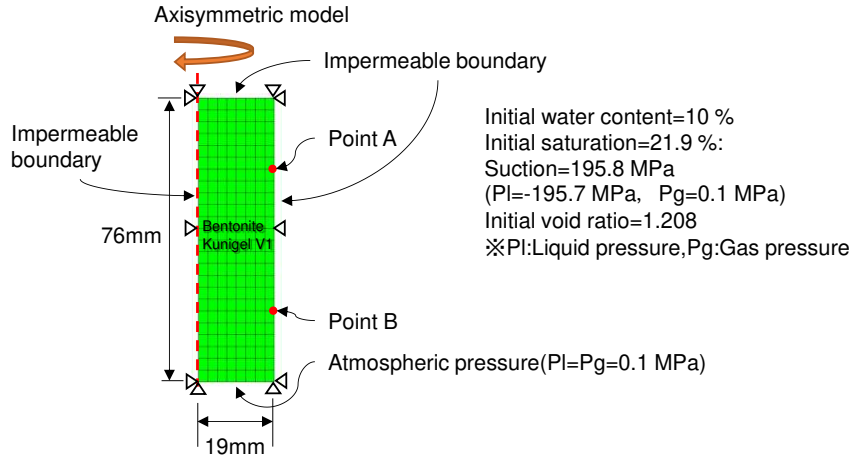

Figure 5. *Model for coupled HM analysis: finite element mesh and initial & boundary conditions, including monitoring points A and B*

3.2.2 Material parameters for two-phase flow properties

The intrinsic permeability K was set using equation (1) (Matsumoto et al., 1997) for the test sample with the dry density $\rho_s = 1.20$ (Mg/m³). The water retention curve was defined with a van Genuchten model (equation (2), van Genuchten,1980) based on that derived for the same bentonite but with dry density $\rho_e = 1.36$ (Mg/m³), as obtained by laboratory experiments (Yamamoto et al., 2019). Here the model parameter related to air entry pressure P_0 was modified considering the dependency on intrinsic permeability as shown in equation (3) (RWMC, 2010). The relative permeabilities were assumed to be described by power law as equation (4) for the gas phase and the van Genuchten model of equation (5) for the liquid phase. It is noted that the residual water saturation S_{lr} is assumed to be zero to fit the water retention and relative permeability curves from related experiments using the van Genuchten model for a relatively higher saturation range.

$$K = \exp(-42.1 + 1.1447\rho_s - 2.1232\rho_s^2) \tag{1}$$

$$P_c = P_0\left(S_e^{n/(1-n)} - 1\right)^{1/n}, S_e = (S_l - S_{lr})/(S_{ls} - S_{lr}) \ , n = 1/(1 - \lambda) \tag{2}$$

$$(P_0)_1 \, / \, (P_0)_2 = (K_1/K_2)^{0.639} \tag{3}$$

$$K_{rg} = A(1 - S_e)^\lambda \tag{4}$$

$$K_{rl} = \sqrt{S_e}\left(1 - \left(1 - S_e^{1/\lambda}\right)^\lambda\right)^2 \ , S_e = (S_l - S_{lr})/(S_{ls} - S_{lr}) \tag{5}$$

where K is intrinsic permeability, ρ_s is dry density, P_c is capillary pressure, P_0 is air entry pressure, S_e is effective saturation, S_l is liquid phase degree of saturation, S_{lr} is residual saturation, S_{ls} is maximum saturation, K_{rg} is gas phase relative permeability, K_{rl} is liquid phase relative permeability and n, λ, A are model parameters.

Figure 6 shows the retention curve and the relative permeability curves used in the analyses. The intrinsic permeability and the model parameters for water retention and relative permeability are shown in Table 1.

3.2.3   Material parameters for mechanical properties

Standard mechanical parameters were defined from previous research results (Yamada et al.,2009). BBM parameters for compression index and swelling index under unsaturated condition are conservatively assumed to be the same as the saturated ones. BBM parameters for swelling deformation were defined from the formula for swelling of bentonite proposed by Komine et al (2003) (Yamamoto et al., 2019). Dependency of tensile strength on suction was considered here. The major mechanical parameters are shown in Table 2.
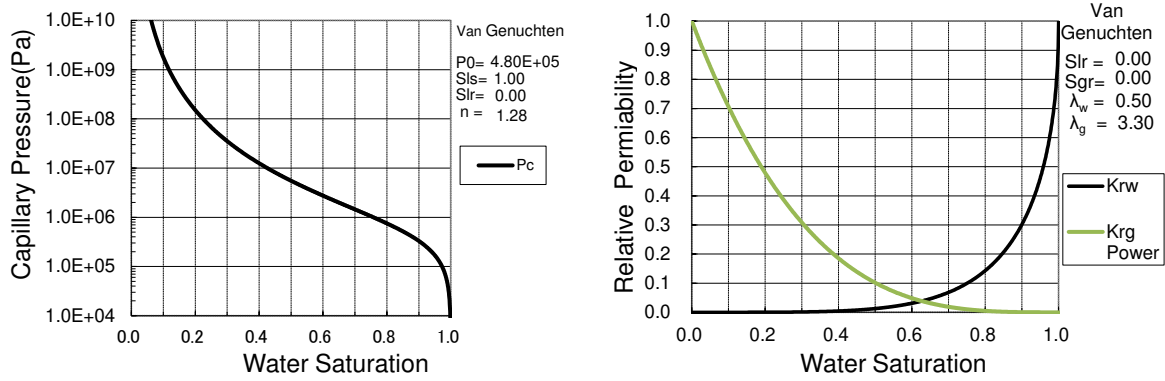

Figure 6. *Water retention curve (left). Relative permeability curve (right)*

Table 1. *Intrinsic permeability and model parameters for two-phase flow*

	Symbol	Unit	Value
Intrinsic Permeability	K	m^3	9.65×10^{-20}
Water retension (van Genuchten model)			
Air entry value parameter	P_0	MPa	0.480
Shape parameter	λ	-	0.218
Residual/ Max water saturation	S_{lr}/S_{ls}	-	0/ 100
Relative permeability for gas phase (Powe model)			
Shape parameter	λ	-	0.500
Residual/ Max water saturation	S_{lr}/S_{ls}	-	0/ 100
Relative permeability for liquid phase (van Genuchten model)			
Shape parameter	λ	-	3.00
Residual/ Max water saturation	S_{lr}/S_{ls}	-	0/ 100

Table 2. *Mechanical parameters for bentonite sample*

Mechanical parameter	Symbol	Unit	Value
Poisson's ratio	α	-	0.30
Slope of void ratio – mean stress curve for saturated material	λ_0	-	0.391
Initial elastic slope for specific volume – mean stress	κ_0	-	0.265
Initial elastic slope for specific volume – suction	κ_{s0}	-	0.111
Parameter for expansive material	α_{sp}	-	0.694
Critical state parameter	M	-	0.338
Initial preconsolidation mean stress for saturated soil	P_0^*	MPa	0.844
Linear constant of increase in tensile strength with suction	k		0.069
Thermal expansion coefficient	α_0	°C^{-1}	2.5×10^{-5}

3.2.4   Thermal parameters for coupled THM analysis

The thermal properties used for THM coupled analysis are shown in Table 3. These are based on the experiments conducted by Kikuchi et al. (2003). Here, thermal conductivity λ varies with saturation according to equation (6).

$$\lambda = \lambda_{sat}\sqrt{S_l} + \lambda_{dry}\left(1 - \sqrt{S_l}\right) \tag{6}$$

where λ_{sat} and λ_{dry} are thermal conductivity in saturated and dry condition respectively and S_l is liquid saturation.

Table 3. *Thermal parameters*

Thermal parameter	Symbol	Unit	Value
Dry thermal conductivity	λ_{dry}	W/m K	1.464
Saturated thermal conductivity	λ_{sat}	W/m K	0.265
Specific heat	C_s	kJ/kg K	0.367

3.3 Numerical results and discussions

3.3.1 Coupled HM analysis

The evolution of pore pressure and porosity with time are shown in Figure 7, for the simulation and laboratory test described above. The pore air pressure evolution up to the peak at the upper monitoring point A (see Figure 5) and up to half of the peak at the lower monitoring point B show good agreement between simulation and measurement. The difference in pore pressure after peak is believed to be caused by the difference in outflow of dissolved air by diffusion due to the difference in the bottom boundary conditions. Out-diffusion at the bottom is not prevented in the analysis, while it is limited in the test due to dissolved air almost saturated in the water supply tube. This could be the reason why the reduction of pore air pressure is much steeper in the analysis than that observed in the test.

The following hypotheses on coupled HM process in bentonite are supported by both the numerical and experimental results (see Figures 7 and 8).

Water absorption by suction in the unsaturated bentonite promotes saturation from the bottom (representing the interface to host rock) toward the top (interface to waste). Pore air in the bentonite is compressed due to the water absorption. This induces gradual development of the air pressure with development of saturation. The air pressure gradient with higher pressure at the top (delayed saturation)
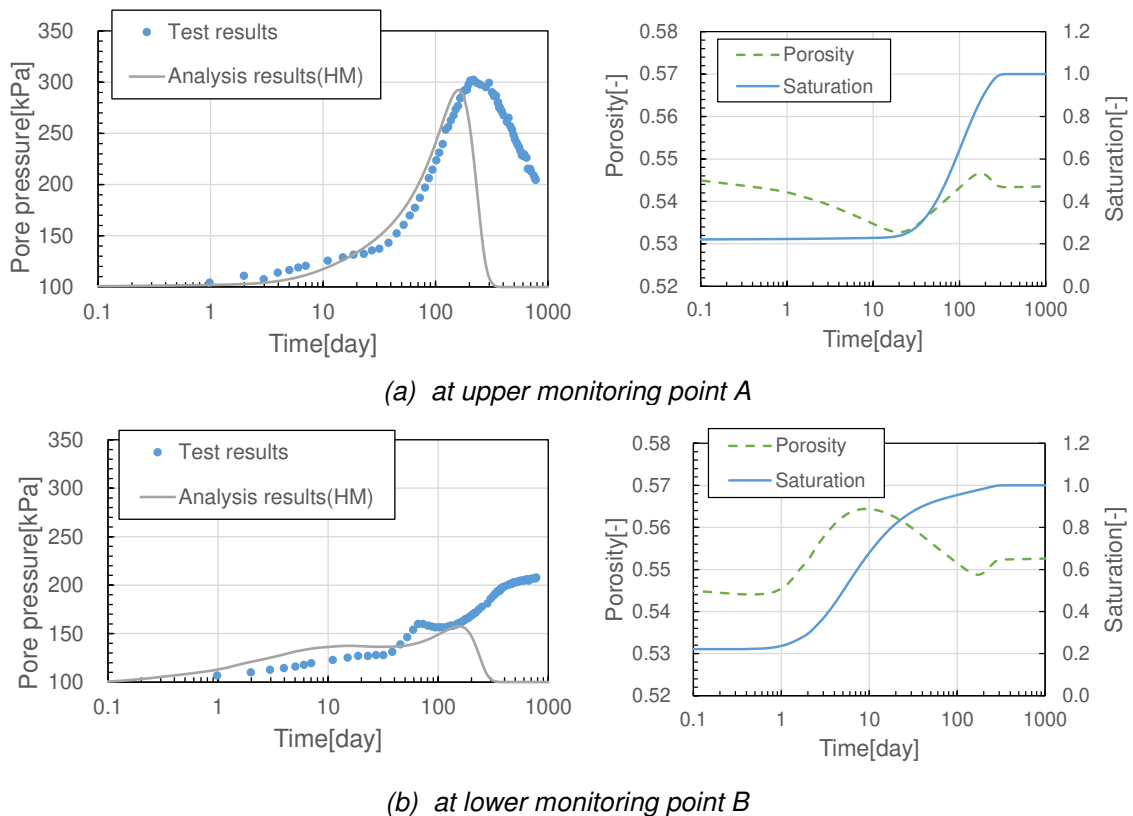

(a) at upper monitoring point A

(b) at lower monitoring point B

Figure 7. *HM coupled analysis result: pressure data from model and laboratory, porosity and saturation from model only*

and lower at the bottom (earlier saturation) occurs according to development of saturation. During the saturation process, the increase in pore pressure doesn't lead to a decrease in saturation ratio even temporarily because of the simultaneous increase in pore pressure.

Advective air flow due to the air pressure gradient towards the bottom end is not possible because of the low air mobility in the saturated lower part of bentonite. Therefore, pore air can only migrate out of the bentonite (EBS) by diffusion of dissolved air in the direction from high concentration/partial pressure (upper part) to lower concentration in the bottom. As the suction of the bentonite decreases with saturation the amount of air decreases by the diffusion over time, and the air pressure reaches a peak after a certain period of time. After the peak pressure, saturation develops quite slowly because of lower suction and lower diffusive flux of the dissolved air to outside. The speed of decrease in pore air pressure after the peak also depends on the flux of dissolved air.
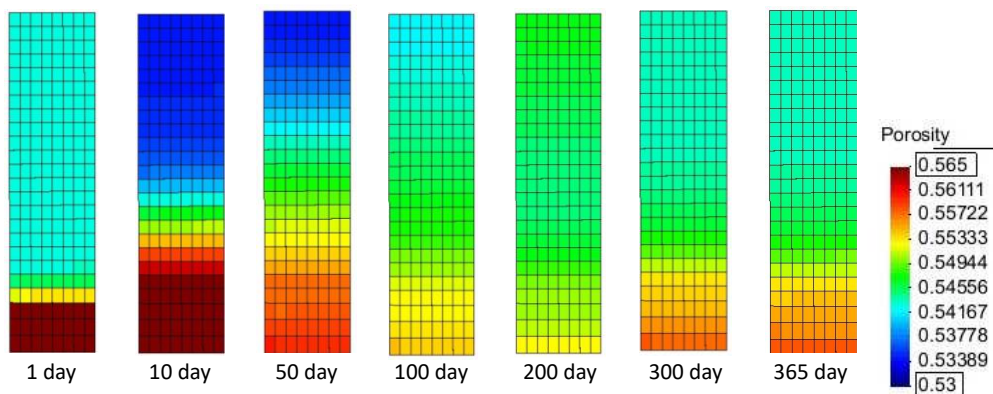
Looking at the simulated change in porosity with time, it increases due to swelling of bentonite in the lower part up to twenty days, while it decreases in the upper part due to the swelling pressure developed
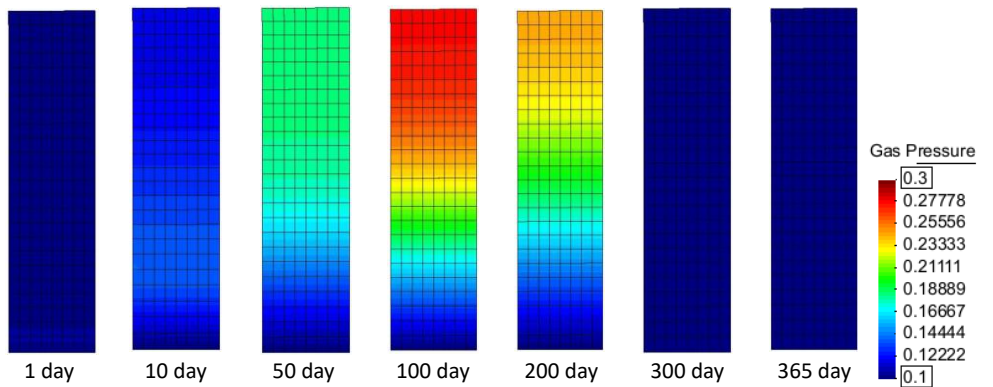
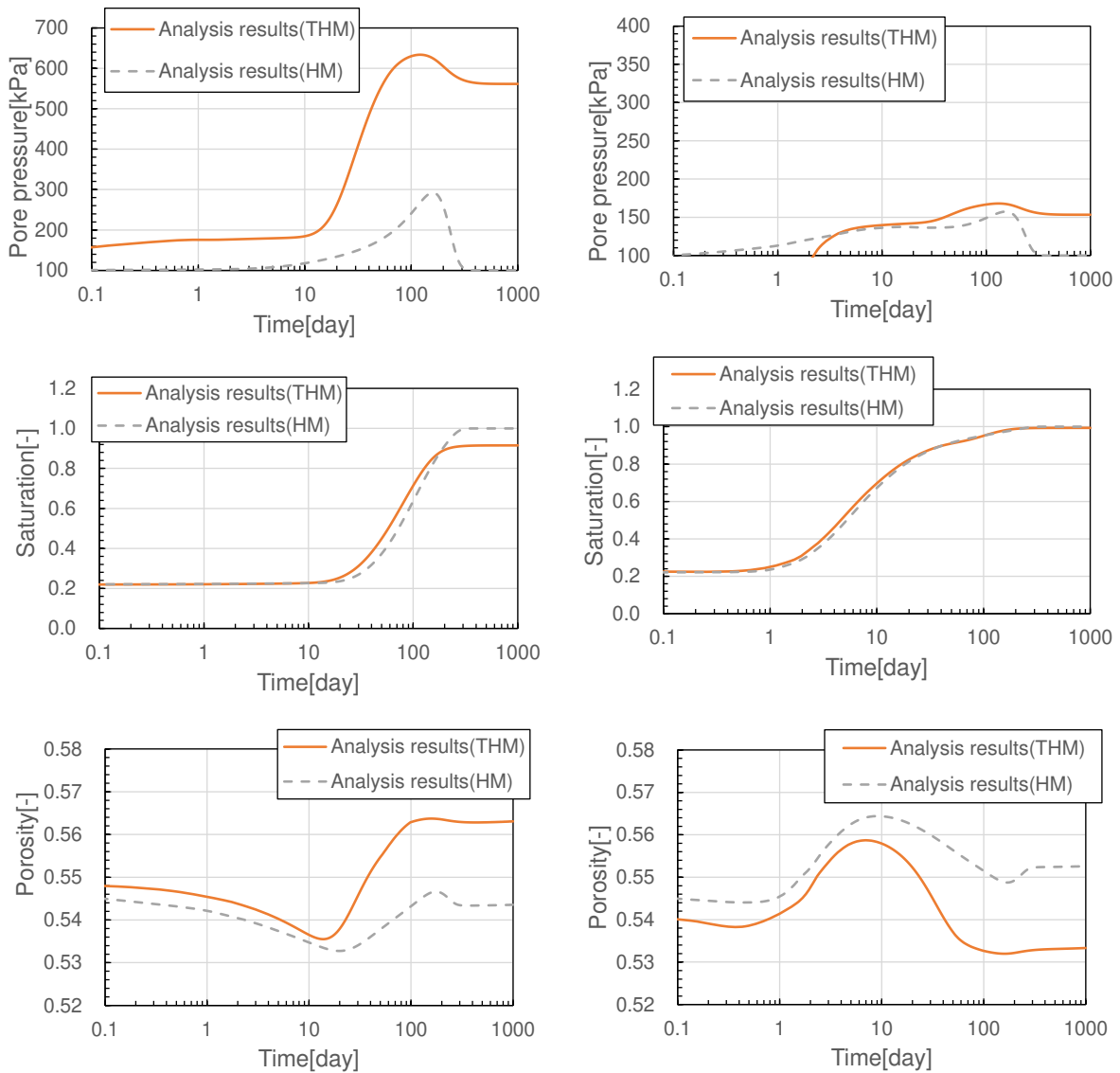(a) Pore air pressure
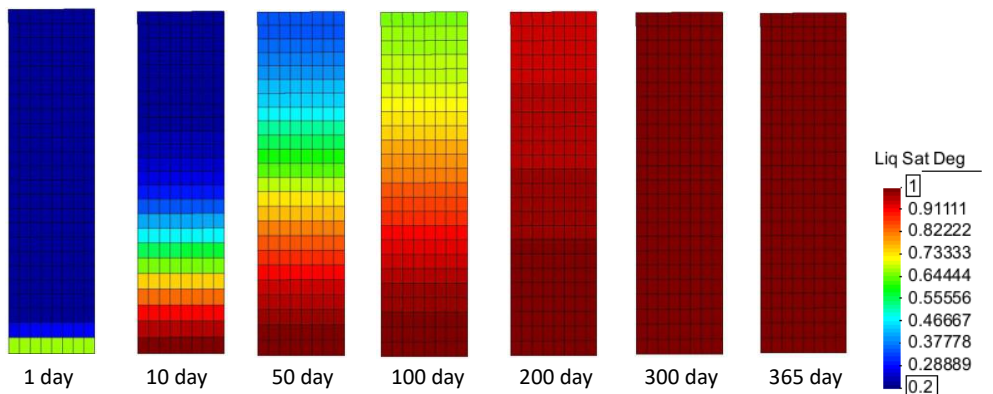
(b) Water saturation

(c) Porosity

Figure 8. Coupled HM analysis results

in the lower part. However, it was confirmed by a two-phase flow analysis without mechanical term that the mechanical effects on both the air pressure evolution and saturation period are negligibly small in this case.

3.3.2   Coupled THM analysis

The results of coupled THM analysis are shown in Figure 9. The following hypotheses on coupled THM process in bentonite are supported by the numerical results. In the THM coupled analysis, the evaporation of pore water in the upper part occurs due to the higher temperature, in addition to dissolution of pore air in water due to the increase in pore air pressure.

The temperature reaches 70 °C after 10 days, and pore air pressure rises faster and to a higher peak than in the coupled HM analysis since the air expands and pore water evaporates due to heating. After the peak pore pressure, pressure stays relatively high. This is not observed in the coupled HM analysis. As evaporation continues to occur by heating while the amount of pore air decreases due to dissolution and diffusion, the pore air pressure doesn't decrease after the peak as steeply as in the coupled HM case (without heating).

(a) at upper monitoring point A   *(b) at lower monitoring point B*

Figure 9. *THM coupled analysis results in comparison to coupled HM analysis*

Regarding mechanical effects, the increase in porosity in the lower part due to swelling in the relatively early period is rather restricted by thermal expansion and vaporization occurring in the upper part, compared with the coupled HM case. On the contrary, the increase in porosity in the upper part is larger due to the same effects. However, it was confirmed by a coupled TH analysis without mechanical term that the mechanical effects on both the air pressure evolution and saturation period are negligibly small in this case.

4   CONCLUSIONS

In this study the coupled THM processes expected in a clay-based engineered barrier material were simulated using a simplified small scale column type cell in both the laboratory and using CODE_BRIGHT. It was clear that pore air in bentonite could play very important role for coupled THM phenomena with e.g. air pressure development due to suction, vaporization and thermal expansion, and then very slow dissipation of the pressure with development of saturation because of restricted advective flow of air and allowable diffusion flow of dissolved air.

The coupled THM process in re-saturation phase in the geological repository should be as follows:
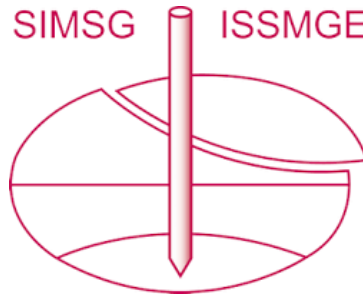
1) Air in the bentonite is compressed due to water intrusion from host rock due to the suction of the unsaturated bentonite. This induces accumulation of the gas pressure. Expansion of pore air and vaporization of pore water by heating from the waste accelerate the pressure development.
2) The air pressure gradient occurs from the upper (waste) part to the lower (rock) side, according to development of water saturation. The temperature gradient amplifies the air pressure gradient. Advective air flow toward the rock is restricted because of the very low air mobility in the saturated bentonite in the vicinity of rock.
3) Therefore, the air can only migrate to the geosphere by diffusion of dissolved air.
4) As the suction of bentonite decreases with evolution of saturation and the amount of the air decreases by diffusion over time, the air pressure reaches a peak after a certain period of time. After the peak saturation develops quite slowly. The accumulated air pressure could not quickly dissipate as the system doesn't allow advective air flow and continuous heating and evaporation occurs in the vicinity of the waste.
5) The void ratio varies locally with time during the saturation process, however mechanical effects to both the air pressure evolution and saturation period are negligibly small if confinement of the barrier material is kept sufficient.

REFERENCES

Alcolea, A., Madaschi, A., Bosch, J. A., Ferrari, A., Laloui, L., Damians, I. P., Olivella, S., Gens, A., Marschall, P., Garitte, B. and Firat-Luthi, B., (2019). The Full-scale Emplacement (FE) Experiment Modeliing Task Force, DECOVALEX Coupled Processes Symposium 2019, Brugg, Switzerland, The DECOVALEX 2019 Project, 18.

Alonso, E. E., Gens, A. and Josa, A. (1990). A constitutive model for partially saturated soils. Ge´otechnique, 40, 405–430. 30).

Garitte, B., Shao, H., Wang, X. R., Nguyen, T. S., Li, Z., Rutqvist, J., Birkholzer, J., Wang, W. Q., Kolditz, O., Pan, P. Z., Feng, X. T., Lee, C., Graupner, B. J., Maekawa, K., Manepally, C., Dasgupta, B., Stothoff, S., Ofoegbu, G., Fedors, R., and Barnichon, J. D. (2017). Evaluation of the predictive capability of coupled thermo-hydro-mechanical models for a heated bentonite/clay system (HE-E) in the Mont Terri Rock Laboratory, Environmental Earth Sciences volume 76, Article number: 64.

Kikuchi, H and Tanai, K. (2003). Heat physical properties examination of buffer material (III) (Testing Document), JNC TN8430, 2003-009. (in Japanese)

Komine, H. and Ogata, N. (2003). New equations for swelling characteristics of bentonite-based buffer materials, Canadian Geotechnical Journal, 40, No. 2, pp.460-475.

Matsumoto, K.,Kanno,T.,Fujita,T. and Suzuki,H. (1997). Saturated permeability of buffer materials. PNC TN8410 97-296.(in Japanese)

Olivella, S., Gens, A., Carrera, J. and Alonso, E. E. (1996). Numerical modelling for a simulator (CODE_BRIGHT) for the coupled analysis of saline media.Engineering Computations, 13, 87–112.

RWMC. (2010). TRU Waste Disposal Technology Development of long-term performance evaluation technology for engineered barriers report (Part 2) -Evaluation of gas migration behavior-. (in Japanese)

van Genuchten and M.Th. (1980) A closed-form equation for predicting the hydraulic conductivity of unsaturated soils, Soil Sci. Soc. Am. J., 44:892-898.

Yamada, A., Adachi, Y., Chijimatsu, M., Amemiya, K., Kaneko, T., Ito, Y., Niwase, K. (2009). Basic property test of bentonite Kunigel GX (Part 4) -Study on static mechanical properties.-, Japan Society of Civil Engineers 2009 Annual Meeting. (in Japanese)

Yamamoto, S., Sato, S., Shimura, T., Romero, E., Nishimura, T. and Owada, H. (2019). Mechanical characteristics and water retention properties of unsaturated "bentonite-based engineered barrier materials" based on controlled-suction tests. Journal of Japan Society of Civil Engineers (JSCE), Vol. 75, No.3, 252-272. (in Japanese)

INTERNATIONAL SOCIETY FOR SOIL MECHANICS AND GEOTECHNICAL ENGINEERING